ICIK
Journal of Intelligent and Sustainable Energy Systems
http://dx.doi.org/10.62762/JISES.2026.737627

RESEARCH ARTICLE

A Chaotic-Adaptive Grey Wolf Optimizer for Sizing Grid-Connected Solar-Wind-Battery Microgrids with EV Fast Charging under Rule-Based Dispatch

Md. Nimul Hasan[1,2,*]

[1] Department of Electrical, Electronic and Communication Engineering, Pabna University of Science and Technology, Rajapur, Pabna 6600, Bangladesh
[2] Department of Electrical and Electronic Engineering, School of Science and Engineering, Uttara University, Dhaka 1230, Bangladesh

Abstract

Fast electric vehicle (EV) charging adds a steep, intermittent load to microgrids built on variable solar and wind generation, and sizing such a microgrid is a non-convex problem. This paper proposes a Chaotic-Adaptive Grey Wolf Optimizer (CAGWO), which modifies the standard Grey Wolf Optimizer (GWO) in two ways: a tent-map chaotic initialization for more even initial coverage, and a nonlinear adaptive convergence factor that extends early exploration. CAGWO sizes the PV, wind, battery, and converter capacities of a grid-connected microgrid supplying an EV fast-charging station. A year-long hourly simulation under a degradation-aware rule-based dispatch evaluates each candidate design, and the objective minimizes net present cost (NPC) under reliability and renewable-fraction limits. For a coastal site in Bangladesh, CAGWO, GWO, particle swarm optimization (PSO), and the whale optimization algorithm (WOA) reach the same design: 1.12 MW PV, 0.49 MW wind, an NPC of US$4.17 million, and a levelized cost of energy of US$0.126/kWh. CAGWO does not lower the final cost relative to GWO (Wilcoxon $p = 0.29$). Its advantage lies in convergence: a lower mean NPC at small iteration budgets and a run-to-run standard deviation of US$17, against more than US$56,000 for GA and WOA. On 30-dimensional benchmarks, CAGWO improves on GWO on all five functions (significant on four), while WOA attains the lowest mean on four of five. The advantage over GWO shrinks to two significant functions at 4 dimensions, and an ablation traces it to the adaptive convergence factor alone. The design rests on one weather year and one EV-demand realization, and scenario-based sizing is left for future work.

Keywords: Grey Wolf Optimizer, chaotic map, adaptive convergence factor, microgrid sizing, electric vehicle fast charging, rule-based dispatch, levelized cost of energy.

Submitted: 27 April 2026
Revised: 24 October 2026
Accepted: 25 October 2026
Published: 23 November 2026

Vol. 1, **No.** 1, 2026.
10.62762/JISES.2026.737627

***Corresponding author:**
✉ Md. Nimul Hasan
nimul34.din.h@gmail.com

Citation
Hasan, M. N. (2026). A Chaotic-Adaptive Grey Wolf Optimizer for Sizing Grid-Connected Solar-Wind-Battery Microgrids with EV Fast Charging under Rule-Based Dispatch. *Journal of Intelligent and Sustainable Energy Systems*, 1(1), 1–17.

© 2026 by the Author. Published by Institute of Central Computation and Knowledge. This is an open access article under the CC BY license (https://creativecommons.org/licenses/by/4.0/).

1 Introduction

Electricity systems are moving toward renewable generation at a pace that reshapes how networks are planned and operated. Global annual additions of renewable capacity were expected to reach roughly 666 GW in 2024, and solar photovoltaic (PV) and wind are forecast to account for the large majority of capacity growth through the end of the decade [1]. Over the same period, electric vehicle (EV) adoption accelerated: more than 17 million electric cars were sold worldwide in 2024, lifting the EV share of new car sales above 20 % for the first time [2]. These two trends are physically linked at the distribution level, where renewable microgrids increasingly host the charging infrastructure that EV fleets depend on. A microgrid that combines local PV, wind, and battery storage can supply an EV charging station with low-carbon energy while reducing stress on the upstream grid, but only if its assets are sized and operated correctly.

The coupling of fast EV charging to renewable generation creates an optimization problem that is harder than conventional microgrid planning. Fast charging draws large, short-duration power pulses whose timing is uncertain and only weakly correlated with solar and wind availability. The planner must size the PV array, wind capacity, battery bank, and converter so that this demand is met at acceptable reliability, while the operator must dispatch the battery hour by hour in a way that respects its degradation limits. Sizing and dispatch are not separable: an undersized battery forces expensive grid imports or unserved load, while an oversized battery inflates capital cost and sits underused. The combined problem is non-convex, high-dimensional, and constrained, with a cost surface shaped by capital recovery, operation and maintenance, time-varying grid tariffs, and battery cycle aging [3, 4]. Classical economic metrics such as net present cost (NPC) and levelized cost of energy (LCOE) summarize the trade-off, and reliability indices such as the loss-of-power-supply probability (LPSP) bound the feasible region [5].

Metaheuristic optimization has become the standard tool for this class of problem because it makes no assumption of convexity or differentiability and scales to mixed sizing-and-dispatch decision vectors. Among the available methods, the Grey Wolf Optimizer (GWO) proposed by Mirjalili et al. [6] is widely used. GWO models the leadership hierarchy and hunting behavior of grey wolves and requires very few control parameters, which makes it simple to implement and tune. It has been applied successfully to optimal power flow [7], multi-microgrid sizing [8], and a broad range of energy problems surveyed by Faris et al. [9]. GWO has also been used to size the battery storage of a microgrid against its operating cost [10], and multi-objective variants extend the method to simultaneous cost, emission, and reliability objectives [9]. For EV charging, Güven et al. [11] sized a hybrid microgrid with charging stations for a small hotel using a quadratic interpolation beluga whale algorithm.

Despite this popularity, the standard GWO carries two structural weaknesses that degrade its performance on the sizing-and-dispatch problem. First, the algorithm initializes its population with uniform random sampling, which gives no guarantee that the initial wolves cover the search space evenly; clusters and gaps in the initial pack bias the early search and waste iterations. Second, the convergence factor that governs the transition from exploration to exploitation decreases linearly with iteration, so the algorithm splits its effort into a fixed exploration half and a fixed exploitation half regardless of the problem landscape [12]. On multimodal cost surfaces, this rigid schedule allows the pack to collapse onto a local optimum before the global region has been located, a failure mode documented across many GWO applications [9].

Two lines of improvement in the literature address these weaknesses. Chaotic maps have been introduced into GWO to replace pseudo-random sequences with deterministic but ergodic sequences: Kohli and Arora studied ten chaotic maps for tuning the control parameter and reported clear gains over standard GWO on constrained benchmarks [13], and tent-map initialization in particular has been used to spread the initial pack more uniformly [14]. In a separate line, nonlinear and adaptive control of the convergence factor has been proposed to rebalance exploration and exploitation; the modified GWO (mGWO) of Mittal et al. [12] replaced the linear decay with a quadratic schedule and improved convergence on engineering problems . Hou et al. [14] combined a tent-map initialization with a nonlinear convergence factor for path planning, but such combinations are usually evaluated on benchmark functions or robotic tasks, and rarely on a coupled microgrid planning problem. The battery degradation cost, which materially changes the dispatch optimum [15, 16], is also frequently omitted from such studies, which weakens the economic relevance of the reported designs.

This paper combines the two lines in a Chaotic-Adaptive Grey Wolf Optimizer (CAGWO) and tests it on the sizing of a renewable microgrid serving an EV fast-charging load. The objective minimizes NPC subject to reliability and renewable-fraction constraints, and LCOE is reported for comparison. The outcome is mixed: on the case study, CAGWO reaches the same design as the standard GWO, PSO, and WOA, so it does not lower the planning cost. Its benefit is faster and more consistent convergence at small iteration budgets, which reduces the computing time of repeated sizing studies. The contributions of this work are as follows.

- A Chaotic-Adaptive Grey Wolf Optimizer (CAGWO) is proposed that integrates tent-map chaotic initialization with a nonlinear adaptive convergence factor, jointly targeting the uneven initialization and rigid exploration–exploitation schedule of the standard GWO.
- The optimizer sizes a grid-connected solar–wind–battery microgrid supplying an EV fast-charging station, with a year-long hourly simulation under a degradation-aware rule-based dispatch.
- CAGWO is verified on standard benchmark functions at 4, 10, and 30 dimensions against GWO, PSO, GA, and WOA, with Wilcoxon rank-sum tests and an ablation of its two modifications. CAGWO improves on GWO, and WOA remains the strongest optimizer at 30 dimensions.
- The method is evaluated on a microgrid case study, with the optimal sizing, NPC and LCOE, dispatch behavior, and a sensitivity analysis on discount rate, EV demand, and grid tariff.

The remainder of this paper is organized as follows. Section 2 describes the microgrid architecture and the component models for PV, wind, battery storage, and the EV charging load. Section 3 states the optimization problem, including the objective function, the economic metrics, and the operating constraints. Section 4 develops the proposed CAGWO, detailing the tent-map initialization, the adaptive convergence factor, and the overall algorithm. Section 5 presents the benchmark verification, the case-study results, and the sensitivity analysis. Section 6 concludes the paper and outlines future work.

2 System Modeling

2.1 Microgrid architecture

The studied system is a grid-connected, AC-coupled microgrid that supplies an EV fast-charging station together with a local base load. Its architecture is shown in Figure 1. A PV array and a battery bank connect to the common AC bus through dedicated power converters, while the wind turbine delivers AC power directly. The utility grid acts as a bidirectional balancing resource: the microgrid imports power when local generation and storage cannot cover demand and exports surplus renewable energy when permitted. An energy management layer, following the rule-based dispatch policy of Section 3.1, coordinates the battery and grid exchange at each time step. The simulation uses an hourly resolution ($\Delta t = 1$ h) over one representative year (8760 h), and the resulting annual operation is extended to the project lifetime through the economic model of Section 3.

2.2 Photovoltaic array model

The PV array output at hour t depends on the incident solar irradiance and the cell temperature [3]:

$$P_{PV}(t) = P_{PV}^{rated}\, f_{PV}\, \frac{G(t)}{G_{STC}} \left[1 + k_T \left(T_c(t) - T_{STC}\right)\right], \tag{1}$$

where P_{PV}^{rated} is the installed PV capacity (a sizing decision variable), f_{PV} is the derating factor that accounts for soiling, wiring losses, and aging, $G(t)$ is the global irradiance on the array plane in W/m^2, $G_{STC} = 1000$ W/m^2 is the irradiance at standard test conditions, k_T is the power temperature coefficient in 1/°C, and $T_{STC} = 25$ °C. The cell temperature $T_c(t)$ is estimated from the ambient temperature $T_a(t)$ using the nominal operating cell temperature (NOCT):

$$T_c(t) = T_a(t) + (NOCT - 20)\, \frac{G(t)}{800}. \tag{2}$$

2.3 Wind turbine model

Measured wind speed at the reference height h_{ref} is translated to the turbine hub height h_{hub} with the power-law profile:

$$v(t) = v_{ref}(t) \left(\frac{h_{hub}}{h_{ref}}\right)^{\gamma}, \tag{3}$$

where γ is the wind shear exponent, taken as $1/7$ for open terrain. The electrical output follows the

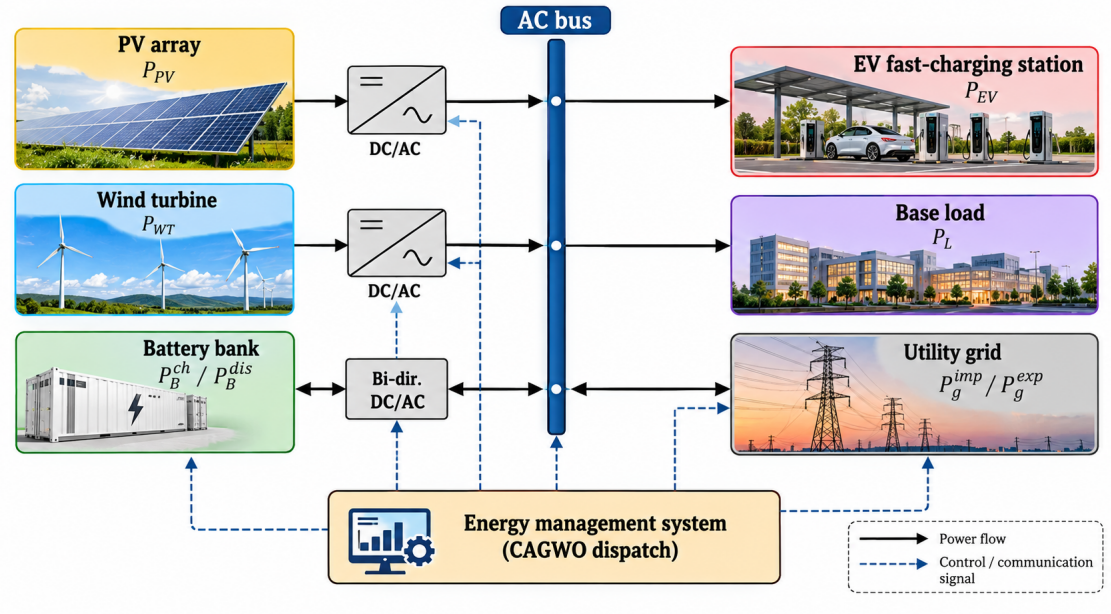

Figure 1. Architecture of the grid-connected solar–wind–battery microgrid supplying an EV fast-charging station and a base load.

piecewise power curve [17]:

$$P_{WT}(t) = \begin{cases} 0, & v(t) < v_{ci} \text{ or } v(t) \geq v_{co}, \\ P_{WT}^{rated} \dfrac{v^3(t) - v_{ci}^3}{v_r^3 - v_{ci}^3}, & v_{ci} \leq v(t) < v_r, \\ P_{WT}^{rated}, & v_r \leq v(t) < v_{co}, \end{cases} \tag{4}$$

where v_{ci}, v_r, and v_{co} are the cut-in, rated, and cut-out speeds, and P_{WT}^{rated} is the installed wind capacity, the second sizing decision variable.

2.4 Battery storage model

The battery bank shifts surplus renewable generation to hours of deficit. Its state of charge (SOC) evolves as

$$SOC(t) = SOC(t-1)\,(1-\sigma) + \left(\eta_{ch} P_B^{ch}(t) - \frac{P_B^{dis}(t)}{\eta_{dis}}\right) \frac{\Delta t}{E_B^{rated}}, \tag{5}$$

where σ is the hourly self-discharge rate, η_{ch} and η_{dis} are the charge and discharge efficiencies, $P_B^{ch}(t)$ and $P_B^{dis}(t)$ are the charge and discharge powers, and E_B^{rated} is the nominal battery capacity, the third sizing decision variable. The SOC and power are bounded by

$$SOC_{min} \leq SOC(t) \leq SOC_{max}, \tag{6}$$

$$0 \leq P_B^{ch}(t) \leq P_B^{max}, \qquad 0 \leq P_B^{dis}(t) \leq P_B^{max}, \tag{7}$$

where $SOC_{min} = 1 - DOD$ is fixed by the allowed depth of discharge DOD (with $SOC_{max} = 1$), and P_B^{max} is set by the battery C-rate. Simultaneous charging and discharging is excluded ($P_B^{ch}(t)\,P_B^{dis}(t) = 0$).

Cycling degrades the battery, and ignoring this cost biases the dispatch toward overuse of storage [15, 16]. A throughput-based degradation cost is therefore charged on every discharged kWh:

$$C_{deg}(t) = \frac{C_B^{cap}}{2\,N_{cyc}(DOD)\,DOD\,\eta_{rt}}\,P_B^{dis}(t)\,\Delta t, \tag{8}$$

where C_B^{cap} is the battery capital cost in US$/kWh, $N_{cyc}(DOD)$ is the cycle life at the operating depth of discharge, and $\eta_{rt} = \eta_{ch}\eta_{dis}$ is the round-trip efficiency. Eq. (8) enters the discharge rule of the dispatch policy in Section 3.1, so the battery is cycled only when the avoided grid cost exceeds the wear it causes.

2.5 Power converter model

The PV array and battery interface the AC bus through converters with efficiency η_{inv}. The PV inverter is assumed to be included in the PV capital cost of Table 1. The converter rating P_C^{rated}, the fourth sizing decision variable, is the battery-interface converter and must carry the largest battery charge or discharge power:

$$P_C^{rated} \geq \max_t \left\{ P_B^{dis}(t),\; P_B^{ch}(t) \right\}. \tag{9}$$

2.6 EV fast-charging load model

The charging station hosts N_{ch} DC fast chargers of rated power P_{ch}^{rated}. Vehicle arrivals in hour t are

modeled as a non-homogeneous Poisson process with hourly rate $\lambda(t)$, which follows a double-peak daily profile, with a morning peak for the commute and an evening peak for the return trip (Figure 6(c)). The double-peak shape is an assumption based on these commuting patterns and is not a measured profile. Open charging-session datasets, such as ACN-Data [18], provide measured arrival-time distributions for calibrating such profiles; ACN-Data covers Level 2 workplace charging rather than DC fast charging, so it is not used directly here. Each session k delivers an energy

$$E_k = (SOC_{dep} - SOC_{arr,k})\, E_{EV,k}, \tag{10}$$

where $SOC_{arr,k}$ is the arrival state of charge, drawn from a truncated normal distribution, SOC_{dep} is the target departure state of charge, and $E_{EV,k}$ is the vehicle battery capacity drawn from the regional EV fleet mix. The aggregate station demand at hour t is

$$P_{EV}(t) = \min\left\{ \sum_{k \in \mathcal{A}(t)} P_{ch}^{rated},\; N_{ch} P_{ch}^{rated} \right\}, \tag{11}$$

where $\mathcal{A}(t)$ is the set of vehicles connected during hour t. Sessions that arrive when all chargers are occupied are queued within the same hour or rolled to the next, which reproduces the demand clustering that makes fast-charging loads difficult to serve from variable generation. One year of synthetic demand $P_{EV}(t)$, $t = 1, \ldots, 8760$, is generated once with a fixed random seed and held identical across all compared algorithms so that performance differences reflect the optimizer alone.

2.7 Grid exchange and power balance

The grid connection is bounded by the interconnection limit P_g^{max} in both directions:

$$0 \le P_g^{imp}(t) \le P_g^{max}, \qquad 0 \le P_g^{exp}(t) \le P_g^{max}. \tag{12}$$

Imports are billed at the time-of-use tariff $c_g(t)$ and exports are credited at the feed-in rate c_{fit}, with $c_{fit} < \min_t c_g(t)$ so that exporting is never preferred over serving local demand. The hourly power balance on the AC bus closes the model:

$$\begin{aligned} &\eta_{inv} P_{PV}(t) + P_{WT}(t) + \eta_{inv} P_B^{dis}(t) \\ &\quad + P_g^{imp}(t) + P_{uns}(t) = P_L(t) + P_{EV}(t) \\ &\quad + \frac{P_B^{ch}(t)}{\eta_{inv}} + P_g^{exp}(t), \end{aligned} \tag{13}$$

where $P_L(t)$ is the base load and $P_{uns}(t) \ge 0$ is unserved power. Unserved energy is not forbidden outright; it accumulates into the loss-of-power-supply probability, which the reliability constraint of Section 3 caps at a prescribed limit. This treatment keeps the search space connected and lets the optimizer trade a marginal reliability shortfall against a large cost saving only within the allowed band.

3 Problem Formulation

3.1 Decision variables and dispatch simulation

The planning problem is a simulation-based sizing optimization. CAGWO searches over the sizing vector

$$\mathbf{x} = \left[P_{PV}^{rated},\; P_{WT}^{rated},\; E_B^{rated},\; P_C^{rated} \right], \tag{14}$$

bounded component-wise by $\mathbf{x}^{min} \le \mathbf{x} \le \mathbf{x}^{max}$. For every candidate $\mathbf{x}$ proposed by CAGWO, the dispatch simulation computes one full year of hourly operation and determines the dispatch variables $\left\{ P_B^{ch}(t), P_B^{dis}(t), P_g^{imp}(t), P_g^{exp}(t), P_{uns}(t) \right\}_{t=1}^{8760}$ subject to the component models and the power balance of Section 2. The dispatch follows a fixed, degradation-aware priority policy and does not optimize the hourly schedule: renewable generation first serves the EV and base loads; any surplus charges the battery until SOC_{max} and is then exported; any deficit is covered by battery discharge when the avoided import cost $c_g(t)$ exceeds the marginal degradation cost of Eq. (8), and by grid import otherwise. This rule couples the operational economics to the sizing decision: a candidate with an oversized battery accumulates degradation cost it cannot recover, while an undersized one pays peak tariffs, and both penalties propagate into the sizing objective.

CAGWO optimizes the four sizing variables only. The rule-based policy fixes the hourly dispatch for a given design, so the reported design is optimal with respect to this policy and not with respect to an optimal dispatch. An optimal dispatch with perfect foresight would lower the operating cost and could shift the optimal battery size. Coupling the sizing with a linear-programming dispatch, and quantifying how the optimal design moves, is left for future work (Section 6).

3.2 Net present cost

The primary objective is the net present cost over the project lifetime of n years at real discount rate i [5, 19]. Annualized economics use the capital recovery factor

$$CRF(i,n) = \frac{i\,(1+i)^n}{(1+i)^n - 1}. \tag{15}$$

The total annualized cost aggregates the four components $j \in \{PV, WT, B, C\}$ together with the operating cash flows:

$$C_{ann} = \sum_{j} \left(C_j^{cap}\, CRF(i,n) + C_j^{rep}\, SFF(i,n_j) + C_j^{OM} \right) + C_{grid} + C_{dem} - R_{exp} + C_{deg}^{yr}, \tag{16}$$

where C_j^{cap} is the capital cost of component j, C_j^{rep} its replacement cost annualized through the sinking fund factor $SFF(i,n_j) = i/[(1+i)^{n_j}-1]$ for a component lifetime $n_j < n$, and C_j^{OM} its annual operation and maintenance cost. The operating terms follow from the simulated year:

$$C_{grid} = \sum_{t=1}^{8760} c_g(t)\, P_g^{imp}(t)\, \Delta t, \qquad R_{exp} = \sum_{t=1}^{8760} c_{fit}\, P_g^{exp}(t)\, \Delta t, \tag{17}$$

$C_{dem} = \sum_{m=1}^{12} c_d \max_{t \in m} P_g^{imp}(t)$ is the annual demand charge with monthly rate c_d, and $C_{deg}^{yr} = \sum_t C_{deg}(t)$ accumulates the battery wear of Eq. (8). The net present cost then follows as

$$NPC(\mathbf{x}) = \frac{C_{ann}}{CRF(i,n)}. \tag{18}$$

3.3 Levelized cost of energy

The levelized cost of energy divides the annualized cost by the energy actually served to the loads:

$$LCOE = \frac{C_{ann}}{\sum_{t=1}^{8760} \left[P_L(t) + P_{EV}(t) - P_{uns}(t) \right] \Delta t}. \tag{19}$$

LCOE is reported alongside NPC because it normalizes designs of different scale and allows direct comparison with grid tariffs and with published charging-station studies [4, 11].

3.4 Reliability constraint

Reliability is measured by the loss-of-power-supply probability, the ratio of unserved to demanded energy over the year [17]:

$$LPSP = \frac{\sum_{t=1}^{8760} P_{uns}(t)\, \Delta t}{\sum_{t=1}^{8760} \left[P_L(t) + P_{EV}(t) \right] \Delta t} \le LPSP_{max}. \tag{20}$$

The cap $LPSP_{max}$ defines the admissible reliability band. A grid-connected station can in principle hold $LPSP = 0$, but enforcing strict zero unserved power forces the interconnection and storage to be sized for the rare coincidence of charger saturation and renewable drought; a small $LPSP_{max}$ avoids sizing for these rare events.

3.5 Renewable fraction

The renewable fraction reports the share of served demand supplied from local renewable resources:

$$RF = 1 - \frac{\sum_{t=1}^{8760} P_g^{imp}(t)\, \Delta t}{\sum_{t=1}^{8760} \left[P_L(t) + P_{EV}(t) - P_{uns}(t) \right] \Delta t}. \tag{21}$$

A floor $RF \ge RF_{min}$ is imposed so that the optimizer cannot degenerate into a grid-only design when import tariffs are low, which would defeat the purpose of the renewable charging station.

3.6 Constrained optimization problem

Collecting the elements above, the sizing problem reads as follows, where Eqs. (1)–(13) are the component models and the power balance, evaluated under the dispatch policy of Section 3.1:

$$\begin{aligned} \min_{\mathbf{x}} \quad & NPC(\mathbf{x}) \\ \text{s.t.} \quad & \text{Eqs. (1)–(13)}, \\ & LPSP \le LPSP_{max}, \qquad RF \ge RF_{min}, \\ & \mathbf{x}^{min} \le \mathbf{x} \le \mathbf{x}^{max}. \end{aligned} \tag{22}$$

Constraint handling uses a static penalty formulation so that every candidate retains a comparable fitness value:

$$F(\mathbf{x}) = NPC(\mathbf{x}) + \rho_1 \max\{0,\ LPSP - LPSP_{max}\} + \rho_2 \max\{0,\ RF_{min} - RF\}, \tag{23}$$

with penalty coefficients ρ_1, ρ_2 set two orders of magnitude above the largest feasible NPC observed in preliminary runs, which keeps infeasible candidates ranked strictly below feasible ones without flattening the ranking information that guides the pack. $F(\mathbf{x})$ is the fitness that CAGWO minimizes in Section 4. The landscape of Eq. (23) is non-convex and multimodal: the piecewise wind power curve Eq. (4), the conditional battery arbitration, and the charger saturation of Eq. (11) all introduce discontinuous derivatives, and discrete tariff bands create plateaus separated by narrow valleys. These are the conditions under which the standard GWO tends to stall (Section 1), and they motivate the chaotic initialization and adaptive convergence schedule developed next [9, 12, 13].

4 Proposed Chaotic-Adaptive Grey Wolf Optimizer

4.1 Standard grey wolf optimizer

The grey wolf optimizer mimics the social hierarchy and hunting strategy of grey wolves [6]. The three fittest candidates are labeled α, β, and δ, and the rest of the pack (ω) follows them. Encircling the prey is modeled as

$$\mathbf{D} = \left|\mathbf{C} \cdot \mathbf{x}_p(t) - \mathbf{x}(t)\right|, \qquad \mathbf{x}(t+1) = \mathbf{x}_p(t) - \mathbf{A} \cdot \mathbf{D}, \tag{24}$$

where $\mathbf{x}_p$ is the prey position and the coefficient vectors are

$$\mathbf{A} = 2a\,\mathbf{r}_1 - a, \qquad \mathbf{C} = 2\,\mathbf{r}_2, \tag{25}$$

with $\mathbf{r}_1, \mathbf{r}_2$ uniform random vectors in $[0, 1]$ and a the convergence factor. Each ω wolf moves under the combined pull of the three leaders:

$$\mathbf{x}(t+1) = \frac{\mathbf{x}_1 + \mathbf{x}_2 + \mathbf{x}_3}{3}, \tag{26}$$

where $\mathbf{x}_1, \mathbf{x}_2, \mathbf{x}_3$ are the positions implied by α, β, δ through Eq. (24). The magnitude of $\mathbf{A}$ governs the search mode: $|\mathbf{A}| \geq 1$ pushes wolves away from the current leaders (exploration), while $|\mathbf{A}| < 1$ pulls them in (exploitation). Since $\mathbf{A}$ scales with a, the schedule of a over iterations controls the exploration–exploitation balance of the whole run.

Two design choices in the standard GWO limit its performance on the non-convex fitness of Eq. (23). The pack is initialized by uniform random sampling, which leaves clusters and gaps in the decision space, and a decreases linearly,

$$a(t) = 2\left(1 - \frac{t}{T}\right), \tag{27}$$

which splits the run into equal exploration and exploitation halves regardless of the landscape [9, 12]. CAGWO replaces both choices.

4.2 Tent-map chaotic initialization

CAGWO seeds the pack with a tent-map chaotic sequence rather than a pseudo-random one. The tent map is ergodic and spreads points more evenly across the unit interval than pseudo-random sampling, which improves the coverage of the initial population [14]. This matters for the small population used here for microgrid sizing. The map is

$$z_{m+1} = \begin{cases} \mu\, z_m, & z_m < 0.5, \\ \mu\,(1 - z_m), & z_m \geq 0.5, \end{cases} \qquad \mu = 1.99. \tag{28}$$

The parameter μ is set to 1.99 instead of 2. At $\mu = 2$, each step of the map shifts one bit out of the binary mantissa, so in double precision the orbit reaches the fixed point $z = 0$: in a test of 1000 random starting values, every orbit at $\mu = 2$ reached zero within 40 to 54 steps. Each sequence starts from $z_0 \in (0, 1) \setminus \{0.5\}$ drawn at random, and the first 100 values are discarded. Over 1000 test initializations (750,000 values at $\mu = 1.99$), no value equals zero or the second fixed point $z^* = \mu/(1+\mu)$, all values are distinct, and they span $[0.00995, 0.995]$, so no orbit collapsed. The chaotic values are mapped to the bounded decision space to set the initial position of wolf i in dimension d:

$$x_{i,d}^{(0)} = x_d^{min} + z_{i,d}\left(x_d^{max} - x_d^{min}\right). \tag{29}$$

Figure 2 contrasts the two schemes for one draw of $N = 25$ wolves. Each dimension takes its own tent sequence, iterated across the wolves; filling the population row-wise from a single sequence would place consecutive coordinates on the graph of the map and collapse the two-dimensional spread onto two lines. With five equal bins per dimension, the coefficient of variation of bin occupancy, averaged over 1000 independent draws at $N = 25$ and $D = 4$, is 0.38 for uniform sampling and 0.31 for the tent map ($p < 10^{-50}$). The tent map therefore spreads the initial pack more evenly; Section 5.1.1 tests whether this changes the final result.

4.3 Nonlinear adaptive convergence factor

CAGWO replaces the linear schedule of Eq. (27) with a nonlinear adaptive factor that holds a high for longer in the early iterations and then drops it quickly:

$$a(t) = (1 - w) \cdot 2\left[1 - \left(\frac{t}{T}\right)^k\right] + w \cdot 2\cos\left(\frac{\pi}{2} \cdot \frac{t}{T}\right). \tag{30}$$

Here $k > 1$ shapes the late-stage decay and $w \in [0, 1]$ blends in a cosine term. With $w = 0$, Eq. (30) crosses $a = 1$ at $t/T = 0.5^{1/k}$, so k sets the length of the exploration phase; with $w = 1$, it reduces to a cosine law crossing $a = 1$ at $t/T = 2/3$. The values $k = 4$ and $w = 0$ were selected by a grid search on the benchmark suite (Table 6), with tuning runs separate from the reported runs. At these values, the exploration phase ($a \geq 1$) lasts 84% of the run, against 50% for the linear law and 71% for the quadratic mGWO law, and the factor then drops steeply into exploitation. Figure 3 compares the schedules.

Table 1. Techno-economic and operating parameters of the case study.

Parameter	Value	Unit
PV capital / O&M cost	900 / 15	US$/kW, US$/kW/yr
Wind capital / O&M cost	1300 / 40	US$/kW, US$/kW/yr
Battery energy capital / O&M	300 / 8	US$/kWh, US$/kW/yr
Battery power capital	200	US$/kW
Converter capital / O&M	300 / 5	US$/kW, US$/kW/yr
Battery replacement / life	300 / 8	US$/kWh, yr
PV derating f_{PV} / coeff. k_T	0.85 / -0.0037	–, 1/°C
Wind v_{ci} / v_r / v_{co}	3 / 12 / 25	m/s
Charge / discharge efficiency	0.95 / 0.95	–
Depth of discharge	0.80	–
Converter efficiency	0.95	–
Project life / discount rate	25 / 0.08	yr, –
Grid limit / feed-in tariff	600 / 0.05	kW, US$/kWh
Demand charge c_d	12	US$/kW/month
ToU tariff (off-peak/base/peak)	0.06 / 0.10 / 0.16–0.22	US$/kWh
Reliability cap $LPSP_{max}$	0.02 (i.e., 2 %)	–
Renewable floor RF_{min}	0.50	–

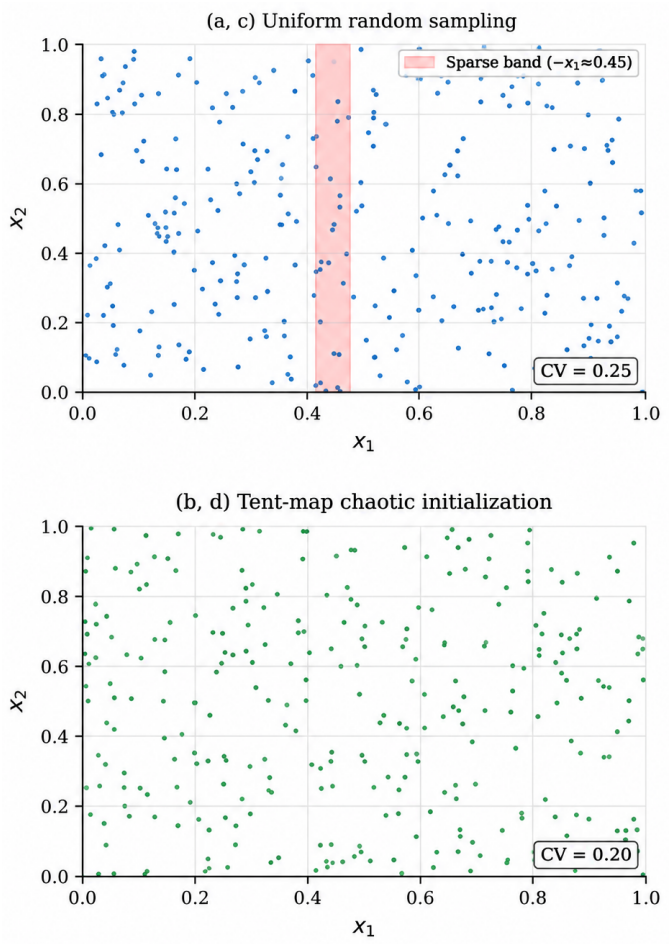

Figure 2. Initial positions of $N = 25$ wolves: (a) uniform random sampling, (b) tent-map initialization.

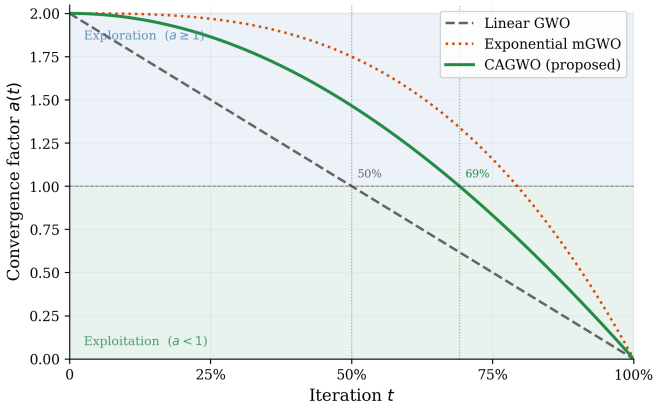

Figure 3. Convergence factor a over iterations for the standard linear GWO, the quadratic mGWO, and the proposed CAGWO ($k = 4$, $w = 0$).

4.4 Algorithm and complexity

Figure 4 shows the complete CAGWO procedure. The tent-map block (Eqs. (28)–(29)) replaces the random seeding, and the adaptive block (Eq. (30)) replaces the linear update of a inside the main loop. Every fitness evaluation calls the dispatch simulation of Section 3, so the cost of one evaluation is set by the 8760-hour annual simulation. With population N and iteration budget T, CAGWO performs $N(T+1)$ fitness evaluations, identical to the standard GWO; the chaotic and adaptive modifications add only $O(NT)$ scalar operations and leave the dominant cost unchanged. CAGWO therefore changes the search behavior at no extra evaluation budget, which is the relevant cost measure when each evaluation is an annual dispatch simulation.

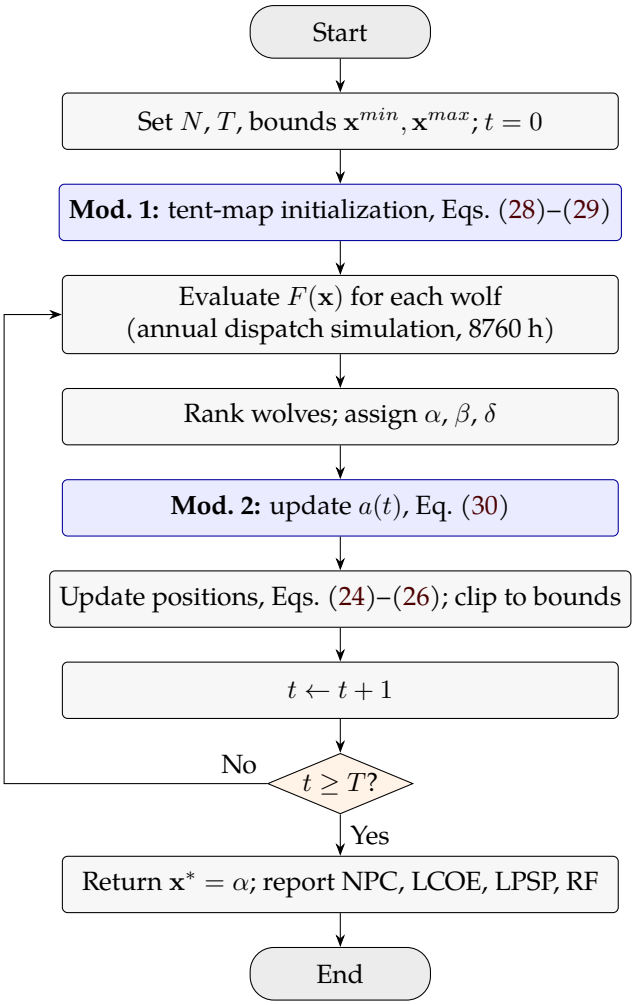

Figure 4. Flowchart of the proposed CAGWO.

5 Results and Discussion

The proposed CAGWO is evaluated in two stages. Section 5.1 verifies the optimizer on standard benchmark functions against the standard GWO, PSO, GA, and WOA. Section 5.2 applies it to the microgrid sizing problem of Sections 2 and 3 for a coastal site in Bangladesh, reporting the optimal design, the dispatch behavior, and a sensitivity analysis. All optimizers use a population of 25. The benchmark runs use 300 iterations and the case study uses 120 iterations, since each case-study evaluation is a full-year dispatch simulation. The techno-economic inputs are listed in Table 1. The ToU tariff of Table 1 is a modeling assumption; for reference, the low-voltage commercial flat rate set by the Bangladesh Energy Regulatory Commission (BERC) from June 2026 is BDT 15.36/kWh (about US$0.124/kWh) [20].

Table 2 lists the control parameters of all five algorithms. All runs share the population size, iteration budget, bounds, and fitness function. Each baseline uses the settings of its source paper or the standard setting in the literature. The benchmark search ranges are $[-100, 100]$ for Sphere, $[-30, 30]$ for Rosenbrock, $[-5.12, 5.12]$ for Rastrigin, $[-32, 32]$ for Ackley, and $[-600, 600]$ for Griewank.

5.1 Benchmark verification

Table 3 reports the results at $D = 30$, the standard setting in the GWO literature.

CAGWO improves on the standard GWO on all five functions. On the Sphere it reaches 3.7×10^{-24} against 1.0×10^{-15} for GWO, nine orders of magnitude lower, and on Ackley it reaches 5.1×10^{-13} against 4.5×10^{-9}. On the strongly multimodal Rastrigin, CAGWO lowers the mean from 16.8 to 9.3 and reaches zero in 2 of 20 runs. The ablation in Section 5.1.1 traces these gains to the adaptive convergence factor.

WOA [24] attains the lowest mean on four of the five functions: Sphere (7.0×10^{-43}), Rosenbrock (16.3), Rastrigin (exact zero in all runs), and Ackley (5.8×10^{-15}). On Griewank, CAGWO has the lower mean (4.0×10^{-3} against 3.6×10^{-2}), but the difference is not significant ($p = 0.31$), and WOA reaches zero in 19 of 20 runs against 15 for CAGWO. On F1 and F4, every WOA run beats every CAGWO run: $p = 6.3 \times 10^{-8}$ is the smallest two-sided rank-sum p-value possible for 20 against 20 runs under the normal approximation, and it marks complete separation of the two samples. On the 30-dimensional suite, WOA therefore outperforms CAGWO. The contribution of CAGWO lies in its improvement over its parent algorithm, GWO, and not in a new best benchmark optimizer. Figure 5 shows the convergence on four functions, where the steeper CAGWO trajectory in the early-to-middle iterations is visible.

The Wilcoxon rank-sum test (Table 4) confirms the improvement over GWO on four functions; on Rosenbrock, both methods reach the same narrow valley, and the difference is not significant ($p = 0.12$). Against PSO and GA, CAGWO is significantly better on all functions. Against WOA, CAGWO is significantly worse on F1, F3, and F4, and the difference is not significant on F2 and F5.

The rank-sum test explains the contrast between F3 and F5 against WOA. WOA reaches exactly zero in all 20 runs on Rastrigin and in 19 of 20 runs on Griewank. On Rastrigin, CAGWO reaches zero in only 2 runs, so 18 stalled CAGWO runs rank above all WOA runs and $p = 1.1 \times 10^{-6}$. All p-values in this section use the normal approximation of the rank-sum statistic without a correction for ties. On Griewank, CAGWO

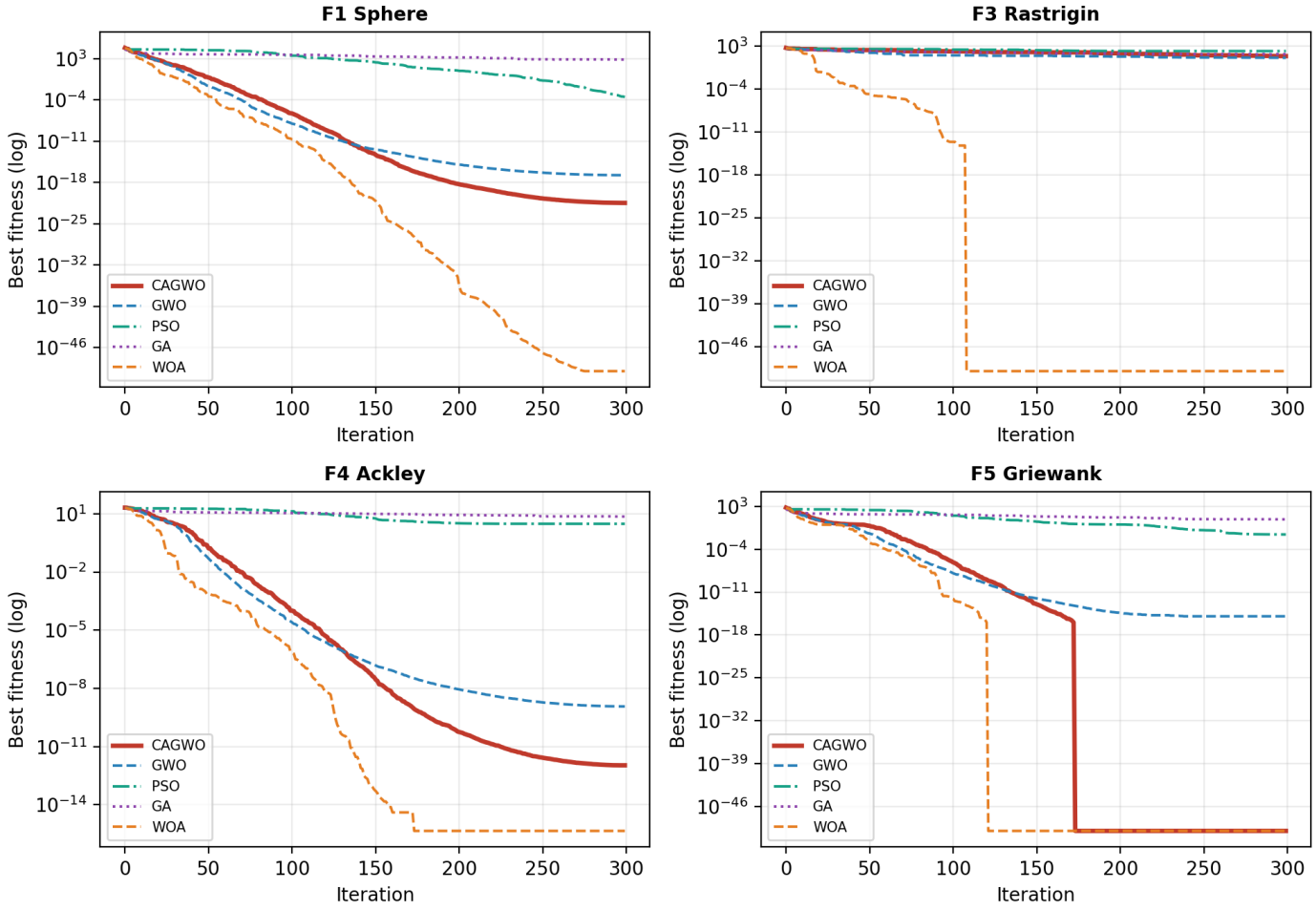

Figure 5. Median best value over 20 runs at $D = 30$ (log scale; zero drawn at 10^{-16}).

reaches zero in 15 of 20 runs. The tied zero runs carry no rank difference, so only the 5 stalled CAGWO runs and the single stalled WOA run separate the samples, which gives $p = 0.31$. With a tie correction, the two values become about 10^{-7} and 0.10, and neither conclusion changes. The means mislead here: one WOA run stalled at a high residual, so the WOA mean (3.6×10^{-2}) exceeds the CAGWO mean (4.0×10^{-3}), while the median of both is zero.

The case-study decision vector holds four variables (Eq. (14)), while the suite above runs at 30 dimensions. To test whether the benchmark gain transfers to the size of the application, the five functions were rerun at $D = 10$ and $D = 4$ with the same population, budget, and 20 runs (Table 5). The advantage over GWO shrinks with dimension: CAGWO is significantly better on four functions at $D = 30$, on three at $D = 10$ (Sphere, Rastrigin, Ackley), and on two at $D = 4$ (Sphere, Ackley). At $D = 4$, the remaining differences fall within run-to-run noise; on Rastrigin, for example, CAGWO reaches zero in all 20 runs and GWO in 15 ($p = 0.18$). The ranking against WOA also changes at low dimension: CAGWO beats WOA on Sphere and Ackley at $D = 4$, and the two are statistically equal on the other three. The trend agrees with the case study, where CAGWO and GWO reach the same design ($p = 0.29$): at low dimension, both algorithms locate the optimum within the budget, and the CAGWO modifications change the speed of convergence more than the final value.

Table 6 reports the grid over $k \in \{1.5, 2, 3, 4\}$ and $w \in \{0, 0.25, 0.5, 0.75, 1\}$, 20 runs per setting at $D = 30$. The settings were ranked by their mean on each function, and the ranks averaged over the five functions. Larger k with small w ranks best, mainly through lower Sphere and Ackley values; the mean Rastrigin value varies between 5.1 and 20.1 with no consistent trend, within the run-to-run spread of the method. The best setting, $k = 4$ and $w = 0$, does not use the cosine term; Eq. (30) then reduces to $a(t) = 2[1 - (t/T)^4]$. Values of k above 4 (6 and 8, tested separately) lowered the Sphere and Ackley values further and gave no consistent change on the other three functions, so the grid was not extended.

Table 2. Control parameters of the compared algorithms.

Algorithm	Parameter	Value
All	Population N	25
	Iterations T (benchmarks / case study)	300 / 120
	Independent runs (benchmarks / case study)	20 / 15
	Boundary handling	clip to bounds
CAGWO	Tent-map parameter μ	1.99
	Discarded transient	100 iterations
	Tent sequences	one per dimension, over the N wolves
	Shape exponent k (Eq. (30))	4
	Cosine weight w (Eq. (30))	0
GWO [6]	Convergence factor a	linear, $2 \rightarrow 0$ (Eq. (27))
PSO [21]	Inertia weight ω	$0.9 \rightarrow 0.4$, linear
	Acceleration c_1, c_2	2.0, 2.0
	Velocity limit	$0.2\,(x^{max} - x^{min})$
GA [22]	Encoding	real-coded
	Selection	binary tournament
	Crossover type / rate	simulated binary [23] ($\eta_c = 20$) / 0.8
	Mutation type / rate	polynomial ($\eta_m = 20$) / $1/D$
	Elitism	2 individuals
WOA [24]	Convergence factor a	linear, $2 \rightarrow 0$
	Spiral constant b	1
	Encircle/spiral switch probability	0.5

Table 3. Benchmark results at $D = 30$: mean $\pm$ standard deviation of the best value over 20 runs ($N = 25$, $T = 300$). Bold: lowest mean per function.

F	Type	CAGWO	GWO	PSO	GA	WOA
F1 Sphere	Uni.	3.7e−24 ± 6.6e−24	1.0e−15 ± 2.5e−15	2.1e+01 ± 1.0e+01	5.2e+01 ± 1.5e+01	**7.0e−43 ± 3.0e−42**
F2 Rosenbrock	Uni.	2.7e+01 ± 5.7e−01	3.7e+01 ± 4.2e+01	1.6e+03 ± 1.7e+03	2.3e+03 ± 1.6e+03	**1.6e+01 ± 1.4e+01**
F3 Rastrigin	Multi.	9.3e+00 ± 1.3e+01	1.7e+01 ± 9.8e+00	7.9e+01 ± 2.6e+01	5.9e+01 ± 1.2e+01	**0 ± 0**
F4 Ackley	Multi.	5.1e−13 ± 4.4e−13	4.5e−09 ± 2.0e−09	2.8e+00 ± 3.9e−01	5.4e+00 ± 2.4e+00	**5.8e−15 ± 3.6e−15**
F5 Griewank	Multi.	**4.0e−03 ± 9.9e−03**	8.4e−03 ± 1.1e−02	1.1e+00 ± 7.4e−02	1.5e+00 ± 1.7e−01	3.6e−02 ± 1.6e−01

Table 4. Wilcoxon rank-sum p-values, CAGWO versus each baseline at $D = 30$. $(+)$ CAGWO significantly better, $(-)$ significantly worse, $(\approx)$ not significant at $p < 0.05$.

Function	vs GWO	vs PSO	vs GA	vs WOA
F1 Sphere	6.3e−08 $(+)$	6.3e−08 $(+)$	6.3e−08 $(+)$	6.3e−08 $(-)$
F2 Rosenbrock	1.2e−01 $(\approx)$	6.3e−08 $(+)$	6.3e−08 $(+)$	5.9e−01 $(\approx)$
F3 Rastrigin	4.5e−03 $(+)$	6.3e−08 $(+)$	8.5e−08 $(+)$	1.1e−06 $(-)$
F4 Ackley	6.3e−08 $(+)$	6.3e−08 $(+)$	6.3e−08 $(+)$	6.3e−08 $(-)$
F5 Griewank	8.0e−04 $(+)$	6.3e−08 $(+)$	6.3e−08 $(+)$	3.1e−01 $(\approx)$
Count $(+/\approx/-)$	4/1/0	5/0/0	5/0/0	0/2/3

5.1.1 Ablation of the two modifications

Table 7 separates the effect of each modification. GWO+T adds only the tent-map initialization, and GWO+A adds only the adaptive convergence factor. The adaptive factor accounts for the whole gain: GWO+A improves significantly on GWO on four functions at $D = 30$ and on two at $D = 4$, the same functions as CAGWO. The tent-map initialization alone changes no function significantly at either dimension ($p \geq 0.24$), and adding it to GWO+A gives no significant change on any function ($p \geq 0.19$). The more even initial spread (bin-occupancy CV 0.31 against 0.38) therefore has no measurable effect on the final solution within a budget of 300 iterations.

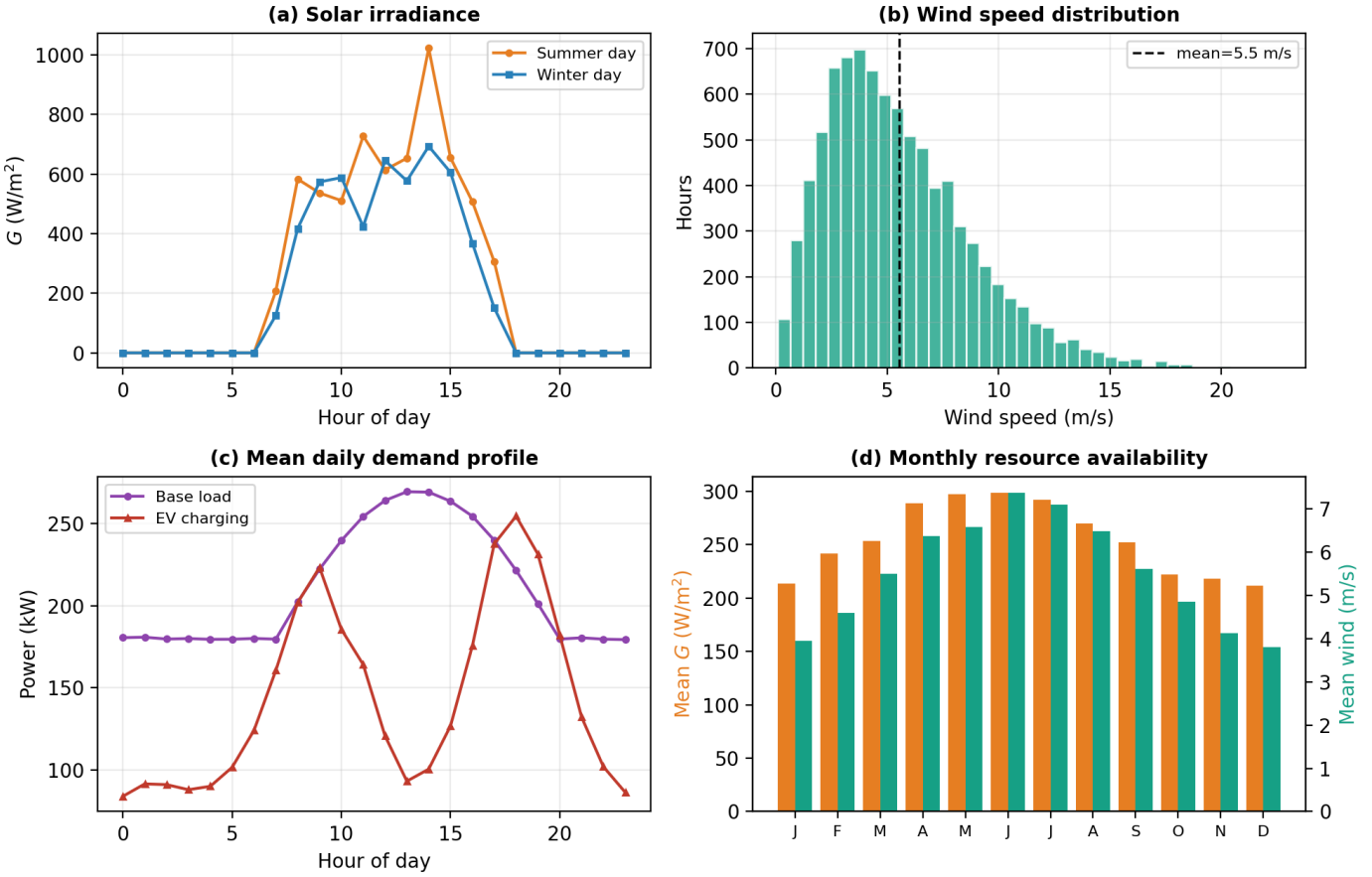

Figure 6. Site input data: (a) solar irradiance on a summer and winter day, (b) annual wind-speed distribution, (c) mean daily base and EV demand, (d) monthly resource availability.

Table 5. Mean $\pm$ standard deviation over 20 runs at $D = 4$ and $D = 10$ ($N = 25$, $T = 300$). Bold: lowest mean. Last two columns: Wilcoxon rank-sum p-value of CAGWO against GWO and WOA, with $(+)$ CAGWO better, $(-)$ worse, $(\approx)$ not significant at $p < 0.05$.

D	F	CAGWO	GWO	PSO	GA	WOA	p vs GWO	p vs WOA
4	F1	**3.3e−102 ± 1.4e−101**	9.3e−71 ± 3.0e−70	6.9e−16 ± 1.5e−15	2.6e−05 ± 2.5e−05	2.8e−51 ± 1.2e−50	6.3e−08 (+)	6.3e−08 (+)
	F2	**9.8e−01 ± 3.0e−01**	1.7e+00 ± 1.7e+00	2.5e+00 ± 5.9e+00	3.4e+00 ± 5.1e+00	2.7e+00 ± 6.5e+00	3.7e−01 (≈)	3.3e−01 (≈)
	F3	**0 ± 0**	7.9e−01 ± 1.5e+00	2.5e−01 ± 4.4e−01	1.9e−04 ± 4.7e−04	8.9e−17 ± 4.0e−16	1.8e−01 (≈)	7.9e−01 (≈)
	F4	**4.4e−16 ± 0**	2.8e−15 ± 1.7e−15	9.6e−09 ± 7.5e−09	4.0e−03 ± 3.3e−03	3.3e−15 ± 2.2e−15	4.4e−04 (+)	1.5e−04 (+)
	F5	**2.6e−02 ± 2.6e−02**	3.2e−02 ± 2.8e−02	4.7e−02 ± 3.9e−02	4.1e−02 ± 2.6e−02	5.1e−02 ± 1.0e−01	5.0e−01 (≈)	1.2e−01 (≈)
10	F1	**7.6e−54 ± 1.0e−53**	1.1e−34 ± 2.6e−34	1.1e−05 ± 1.5e−05	2.9e−02 ± 1.8e−02	1.2e−48 ± 3.3e−48	6.3e−08 (+)	5.0e−05 (+)
	F2	6.6e+00 ± 4.1e−01	6.6e+00 ± 7.1e−01	1.7e+01 ± 2.5e+01	1.1e+02 ± 3.6e+02	**3.6e+00 ± 4.0e+00**	8.1e−01 (≈)	1.0e−01 (≈)
	F3	2.8e+00 ± 7.0e+00	6.9e+00 ± 7.6e+00	7.5e+00 ± 2.5e+00	9.3e−01 ± 5.7e−01	**0 ± 0**	6.5e−04 (+)	1.8e−01 (≈)
	F4	**4.0e−15 ± 0**	1.2e−14 ± 3.4e−15	1.0e−03 ± 1.0e−03	8.3e−02 ± 4.0e−02	4.5e−15 ± 2.4e−15	6.3e−08 (+)	4.2e−01 (≈)
	F5	**4.3e−02 ± 7.7e−02**	4.5e−02 ± 6.9e−02	1.8e−01 ± 1.2e−01	1.3e−01 ± 6.1e−02	4.7e−02 ± 1.4e−01	5.9e−01 (≈)	8.7e−03 (−)

Table 6. Sensitivity of CAGWO to k and w ($D = 30$, 20 tuning runs per cell, seeds separate from Table 3). Each cell: mean rank over F1–F5 among the 20 settings (lower is better) / mean Rastrigin value. Bold: selected setting.

$k \setminus w$	0	0.25	0.5	0.75	1
1.5	16.0 / 15.5	17.2 / 14.1	17.0 / 15.2	14.8 / 12.6	9.8 / 11.6
2	12.0 / 15.5	14.8 / 20.1	8.0 / 10.5	12.2 / 9.2	9.8 / 11.6
3	4.6 / 6.5	9.2 / 8.8	8.0 / 7.3	9.6 / 10.2	9.8 / 11.6
4	**2.6 / 7.1**	6.2 / 5.1	9.4 / 6.8	7.2 / 8.4	9.8 / 11.6
Exploration share ($w = 0$): k=1.5: 63%, k=2: 71%, k=3: 79%, k=4: 84%					

Table 7. Ablation: mean over 20 runs. GWO+T: tent-map initialization only; GWO+A: adaptive convergence factor only. In brackets: rank-sum p-value against GWO. Bold: $p < 0.05$.

D	F	GWO	GWO+T	GWO+A	CAGWO
30	F1	1.0e−15	9.1e−16 (7.3e−01)	**2.7e−24 (6.3e−08)**	**3.7e−24 (6.3e−08)**
	F2	3.7e+01	2.7e+01 (8.1e−01)	2.7e+01 (2.7e−01)	2.7e+01 (1.2e−01)
	F3	1.7e+01	2.7e+01 (8.9e−01)	**4.9e+00 (1.5e−04)**	**9.3e+00 (4.5e−03)**
	F4	4.5e−09	4.2e−09 (7.7e−01)	**4.9e−13 (6.3e−08)**	**5.1e−13 (6.3e−08)**
	F5	8.4e−03	7.2e−03 (5.2e−01)	**2.4e−03 (7.1e−06)**	**4.0e−03 (8.0e−04)**
4	F1	9.3e−71	1.1e−70 (7.0e−01)	**7.5e−104 (6.3e−08)**	**3.3e−102 (6.3e−08)**
	F2	1.7e+00	1.2e+00 (2.4e−01)	1.9e+00 (6.7e−01)	9.8e−01 (3.7e−01)
	F3	7.9e−01	2.0e−01 (3.9e−01)	4.8e−01 (4.8e−01)	0 (1.8e−01)
	F4	2.8e−15	2.0e−15 (2.8e−01)	**4.4e−16 (4.4e−04)**	**4.4e−16 (4.4e−04)**
	F5	3.2e−02	4.1e−02 (9.1e−01)	3.0e−02 (2.3e−01)	2.6e−02 (5.0e−01)

5.2 Microgrid case study

The optimizer is applied to the coastal site, whose resource and demand profiles are shown in Figure 6. The site combines strong midday irradiance with a mean wind speed near 5.5 m/s and a double-peak EV charging demand superimposed on a daytime-heavy base load. These hourly series drive the dispatch simulation for every candidate design.

Table 8 reports the optimal sizing and economics found by each algorithm. CAGWO, GWO, PSO, and WOA all converge to the same design within rounding: a PV-dominant system of about 1.12 MW PV and 0.49 MW wind with the battery driven to its lower bound. Under the assumed tariffs and the grid connection, large storage is uneconomic, so the optimizer meets the reliability target with renewables plus controlled grid exchange and a minimal battery, while the annual demand charge of US$86,000 implies a monthly billed import peak near the 600 kW grid limit. The resulting NPC is about US$4.17 million with an LCOE of US$0.126/kWh, an LPSP of 0.02 % (against the 2 % cap), and a renewable fraction of 66 %, all within the imposed limits.

Table 8. Optimal sizing and economics by algorithm (best of 15 runs); mean and standard deviation of the converged NPC across runs.

Quantity	CAGWO	GWO	PSO	GA	WOA
PV (kW)	1119	1113	1112	1106	1109
Wind (kW)	491	491	490	503	492
Battery (kWh)	100	100	100	116	100
Converter (kW)	100	100	100	163	100
Bat. power (kW)	50	50	50	123	50
NPC (M US$)	4.170	4.170	4.170	4.220	4.170
LCOE (US$/kWh)	0.1258	0.1258	0.1258	0.1273	0.1258
LPSP (%)	0.019	0.019	0.019	0.024	0.019
RF (%)	66.1	66.1	66.0	67.1	66.0
Mean NPC (M US$)	4.1697	4.1696	4.1696	4.277	4.224
Std NPC (US$)	17	18	11	56841	61222

The case study separates the algorithms on robustness rather than on the best design. CAGWO, GWO, and PSO converge to the optimum on every run, with standard deviations of US$17, US$18, and US$11 across 15 runs; the three are equally reliable at the full budget. GA and WOA are far less reliable, with standard deviations above US$56,000 and mean NPCs that exceed the optimum by 2.6 % and 1.3 %; GA fails to reach the optimal region within the budget on several runs, and WOA occasionally stalls on a costlier design. A Wilcoxon rank-sum test on the converged NPC confirms that CAGWO and the standard GWO are statistically indistinguishable on this problem ($p = 0.29$), while CAGWO significantly outperforms GA ($p = 3.1 \times 10^{-6}$) and WOA ($p = 5.3 \times 10^{-4}$). The smooth, strongly attracting optimum of this grid-connected design is reached by all competent metaheuristics, so the practical value of CAGWO here is its reliable, fast convergence rather than a lower final cost.

That convergence advantage is visible in Figure 7. Panel (a) shows the best-run trajectories: CAGWO, GWO, PSO, and WOA collapse onto the optimum within the first iterations, while GA descends slowly. Panel (b) plots the mean best-so-far against the iteration budget over all 15 runs. At a tight budget of five iterations CAGWO already reaches US$4.19 M, ahead of the standard GWO at US$4.20 M, and by 20 iterations the two are within US$1000 of the optimum; GA and WOA need far more iterations and never fully close the gap. Sizing is an offline problem, solved once per planning study, so for a single run the faster convergence of CAGWO carries limited weight. All five algorithms perform the same $N(T +$

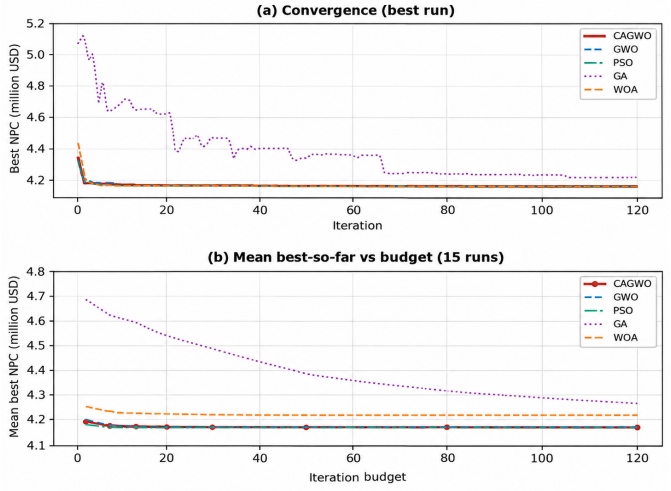

Figure 7. Case-study convergence: (a) best-run NPC trajectories, (b) mean best-so-far NPC versus iteration budget over 15 runs.

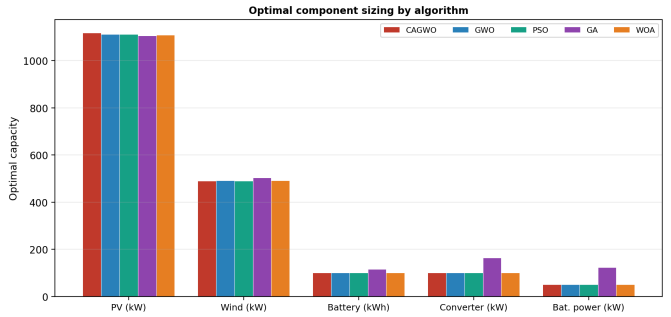

Figure 8. Optimal component sizing by algorithm. The four reliable methods agree closely; GA converges to a heavier, costlier design.

1) = 3025 fitness evaluations per run, each one an annual dispatch simulation, so the computing cost per run is identical. The convergence advantage matters when the sizing problem is solved many times, as in the sensitivity analysis of Section 5.3, where each point is an independent re-optimization; there, a smaller iteration budget per re-optimization suffices. A measurement of wall-clock time and of the saving in large repeated studies is left for future work.

The optimal sizing is compared across algorithms in Figure 8, which shows the close agreement among the four reliable methods and the heavier, costlier configuration that GA settles on. The annualized cost composition of the CAGWO design is shown in Figure 9(a): the annualized capital of US$161,000 dominates, followed by the grid-import bill of US$140,000 and the demand charge of US$86,000, with battery degradation contributing only US$3,300 because the optimal battery is small. Export revenue offsets about US$41,000. Panel (b) confirms that NPC and LCOE are near-identical across the four reliable

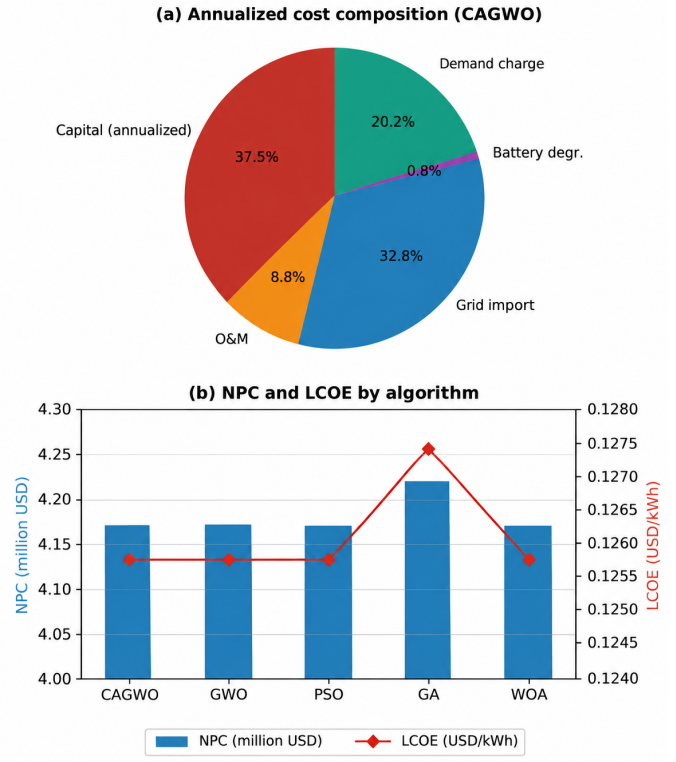

Figure 9. (a) Annualized cost composition of the CAGWO design. (b) NPC and LCOE by algorithm.

algorithms and higher for GA.

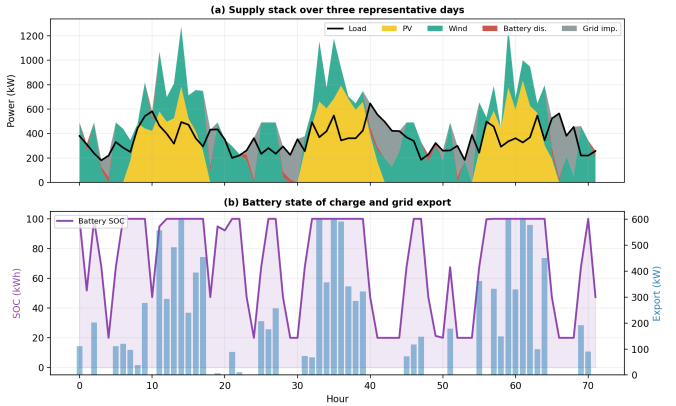

Figure 10. Dispatch of the CAGWO-optimized microgrid over three representative days: (a) supply stack against load, (b) battery state of charge and grid export.

Figure 10 illustrates the dispatch of the CAGWO design over three representative summer days. Panel (a) shows PV carrying the midday load while wind contributes through the day and night, with grid import filling the residual and the small battery smoothing short deficits. Panel (b) shows the battery cycling between its bounds and surplus renewable energy being exported around midday. The design serves the double-peak EV demand without violating the reliability cap, which indicates that the sizing and

the embedded dispatch policy are consistent.

5.3 Sensitivity analysis

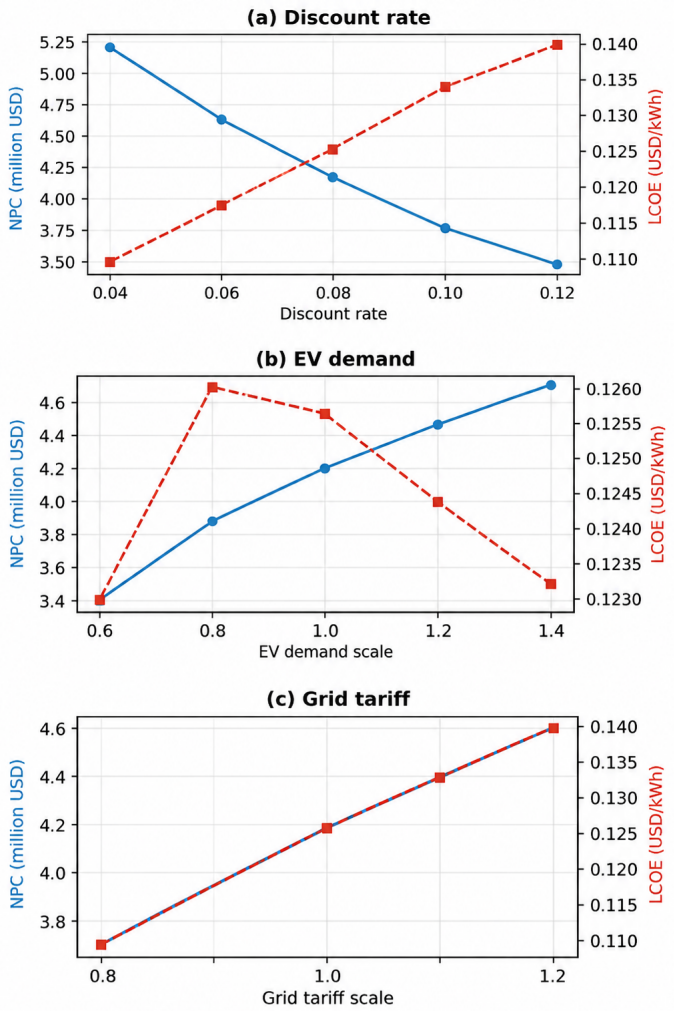

Figure 11. Sensitivity of the CAGWO-optimized NPC and LCOE to (a) discount rate, (b) EV demand scale, and (c) grid tariff scale.

The robustness of the design to economic and demand assumptions is examined by re-optimizing with CAGWO while varying one factor at a time. Figure 11 reports the results. A higher discount rate lowers the NPC, since future operating costs are discounted more heavily, but raises the LCOE because annualized capital carries more weight; across the range 0.04 to 0.12 the NPC falls from US$5.2 M to US$3.5 M. Scaling the EV demand from 0.6 to 1.4 of the nominal raises the NPC monotonically from US$3.4 M to US$4.7 M, while the LCOE varies only mildly because the larger served energy spreads the fixed costs. Scaling the grid tariff from 0.7 to 1.3 raises both the NPC and the LCOE almost linearly, since grid import is a standing share of the annual cost. The optimal mix stays PV-dominant across all sensitivity cases. The NPC responds most to the discount rate, a financing assumption, and among the design-relevant inputs, to the EV demand.

5.4 Discussion

The benchmark and case-study results agree. On the benchmark suite, where landscapes are deliberately rugged, the adaptive convergence schedule gives CAGWO a clear and statistically significant edge over the standard GWO and over PSO and GA, while WOA remains significantly stronger on three of the five functions at 30 dimensions. On the grid-connected microgrid, where the feasible cost surface has a single strong optimum, that edge narrows: CAGWO matches the best metaheuristics on the final design and distinguishes itself through fast, reliable convergence and low run-to-run variance, clearly outperforming GA and WOA. For a planner, this means CAGWO returns the cost-optimal design with a small iteration budget, which matters when each evaluation is a full-year dispatch simulation.

The reported sizing rests on one representative weather year and one realization of the EV arrival process, generated with a fixed seed so all algorithms face the same demand. The design is therefore specific to this scenario. The sensitivity analysis indicates a stable PV-dominant structure under scaled EV demand, tariff, and discount rate, but it does not replace a test across years of weather data and independent realizations of EV arrivals, under which the exact capacities may shift. Scenario-based sizing of this kind is left for future work, together with measured resource and charging data for the site.

6 Conclusion

This paper tested a Chaotic-Adaptive Grey Wolf Optimizer (CAGWO) for sizing a grid-connected solar–wind–battery microgrid with an EV fast-charging station under a degradation-aware rule-based dispatch. The main findings are as follows. First, CAGWO improves on its parent GWO, significantly on four of five benchmark functions at 30 dimensions, but WOA remains significantly stronger on three of them, and the gain over GWO shrinks to two functions at the 4-dimensional size of the sizing problem. The ablation attributes the gain to the adaptive convergence factor; the tent-map initialization spreads the initial pack more evenly without a measurable effect on the final result. Second, on the case study, CAGWO, GWO, PSO, and WOA reach the same design (1.12 MW PV, 0.49 MW wind, minimal storage), so the choice among competent optimizers does not change the planning outcome for

this grid-connected system. The value of CAGWO lies in convergence: it reaches a near-optimal design within a few iterations and with low run-to-run spread, which helps when the sizing is repeated many times, as in sensitivity studies. Third, the design keeps its PV-dominant structure across the sensitivity sweeps of discount rate, EV demand, and grid tariff.

The results carry two implications for Bangladesh. The levelized cost of US$0.126/kWh lies close to the low-voltage commercial flat tariff of BDT 15.36/kWh (about US$0.124/kWh) and about 37% above the battery-charging-station tariff of BDT 11.36/kWh (about US$0.092/kWh), both set by BERC from June 2026 [20], at an exchange rate of about BDT 123.4 per US dollar. A renewable charging station of this design therefore does not undercut the regulated charging tariff, in a power sector where a deficit of about BDT 410 billion (41,000 crore) is still projected after the increase. Its case rests on the 66% renewable fraction, which is above the national targets of 20% renewable electricity by 2030 and 30% by 2040 under the Renewable Energy Policy 2025 [25], although a site-level share and a national generation share are not directly comparable. Charging stations built as renewable microgrids can contribute toward these targets, provided tariff design or net-metering credits close the gap of about US$0.03/kWh.

The study has limitations, which define the future work. The design rests on one site, one representative weather year, and one realization of EV arrivals; scenario-based sizing across years of weather data and independent EV-demand realizations, with measured resource and fast-charging data, is the first next step. The dispatch is rule-based; coupling the sizing with an optimal linear-programming dispatch would show how far the rule-based design lies from the optimum. The computing benefit of faster convergence should be measured in wall-clock time over large repeated studies. Finally, CAGWO can be extended to a multi-objective form trading cost against emissions and reliability.

Data Availability Statement

The data used to support the findings of this study are available from the corresponding author upon request.

Funding

This work was supported without any funding.

Conflicts of Interest

The author declares no conflicts of interest.

AI Use Statement

The author declares that no generative AI was used in the preparation of this manuscript.

Ethical Approval and Consent to Participate

Not applicable.

References

[1] International Energy Agency. (2024). Renewables 2024: Analysis and forecast to 2030. IEA, Paris. Retrieved from https://www.iea.org/reports/renewables-2024

[2] International Energy Agency. (2025). Global EV Outlook 2025. IEA, Paris. Retrieved from https://www.iea.org/reports/global-ev-outlook-2025

[3] Ishraque, M. F., Shezan, S. A., Ali, M. M., & Rashid, M. M. (2021). Optimization of load dispatch strategies for an islanded microgrid connected with renewable energy sources. *Applied Energy, 292*, 116879. [CrossRef]

[4] Ul Hassan, S., Yousif, M., Nawaz Khan, S., Kazmi, S. A. A., & Imran, K. (2023). A decision-centric approach for techno-economic optimization and environmental assessment of standalone and grid-integrated renewable-powered electric vehicle charging stations under multiple planning horizons. *Energy Conversion and Management, 294*, 117571. [CrossRef]

[5] Alharbi, A. M., Ali, Z. M., & Zaki Diab, A. A. (2025). Comparative techno-economic optimization of microgrid configurations using hybrid battery–hydrogen storage: NEOM case study, Saudi Arabia. *PLOS ONE, 20*(9), e0326050. [CrossRef]

[6] Mirjalili, S., Mirjalili, S. M., & Lewis, A. (2014). Grey wolf optimizer. *Advances in Engineering Software, 69*, 46-61. [CrossRef]

[7] El-Fergany, A. A., & Hasanien, H. M. (2015). Single and multi-objective optimal power flow using grey wolf optimizer and differential evolution algorithms. *Electric Power Components and Systems, 43*(13), 1548-1559. [CrossRef]

[8] Aeggegn, D. B., Nyakoe, G. N., & Wekesa, C. (2024). Optimal sizing of grid connected multi-microgrid system using grey wolf optimization. *Results in Engineering, 23*, 102421. [CrossRef]

[9] Faris, H., Aljarah, I., Al-Betar, M. A., & Mirjalili, S. (2018). Grey wolf optimizer: a review of recent variants and applications. *Neural Computing and Applications, 30*(2), 413-435. [CrossRef]

[10] Sharma, S., Bhattacharjee, S., & Bhattacharya, A.

(2016). Grey wolf optimisation for optimal sizing of battery energy storage device to minimise operation cost of microgrid. *IET Generation, Transmission & Distribution, 10*(3), 625-637. [CrossRef]

[11] Güven, A. F., Hassan, M. H., & Kamel, S. (2025). Optimization of a hybrid microgrid for a small hotel using renewable energy and EV charging with a quadratic interpolation beluga whale algorithm. *Neural Computing and Applications, 37*(5), 3973-4008. [CrossRef]

[12] Mittal, N., Singh, U., & Sohi, B. S. (2016). Modified grey wolf optimizer for global engineering optimization. *Applied Computational Intelligence and Soft Computing, 2016*(1), 7950348. [CrossRef]

[13] Kohli, M., & Arora, S. (2018). Chaotic grey wolf optimization algorithm for constrained optimization problems. *Journal of Computational Design and Engineering, 5*(4), 458-472. [CrossRef]

[14] Hou, Y., Gao, H., Wang, Z., & Du, C. (2022). Improved grey wolf optimization algorithm and application. *Sensors, 22*(10), 3810. [CrossRef]

[15] Xu, B., Oudalov, A., Ulbig, A., Andersson, G., & Kirschen, D. S. (2018). Modeling of lithium-ion battery degradation for cell life assessment. *IEEE Transactions on Smart Grid, 9*(2), 1131-1140. [CrossRef]

[16] Fallahifar, R., & Kalantar, M. (2023). Optimal planning of lithium ion battery energy storage for microgrid applications: Considering capacity degradation. *Journal of Energy Storage, 57*, 106103. [CrossRef]

[17] Yang, H., Zhou, W., Lu, L., & Fang, Z. (2008). Optimal sizing method for stand-alone hybrid solar–wind system with LPSP technology by using genetic algorithm. *Solar Energy, 82*(4), 354-367. [CrossRef]

[18] Lee, Z. J., Li, T., & Low, S. H. (2019, June). ACN-data: Analysis and applications of an open EV charging dataset. In *Proceedings of the Tenth ACM International Conference on Future Energy Systems* (pp. 139-149). [CrossRef]

[19] Kumar, J., Suryakiran, B. V., Verma, A., & Bhatti, T. S. (2019). Analysis of techno-economic viability with demand response strategy of a grid-connected microgrid model for enhanced rural electrification in Uttar Pradesh state, India. *Energy, 178*, 176-185. [CrossRef]

[20] Bangladesh Energy Regulatory Commission. (2026). Retail electricity tariff order, effective from the June 2026 billing month. BERC, Dhaka. Retrieved from https://berc.org.bd

[21] Kennedy, J., & Eberhart, R. (1995, November). Particle swarm optimization. In *Proceedings of ICNN'95 - International Conference on Neural Networks* (Vol. 4, pp. 1942-1948). IEEE. [CrossRef]

[22] Holland, J. H. (1975). *Adaptation in natural and artificial systems*. University of Michigan Press. https://archive.org/details/adaptationinnatu0000holl/mode/2up

[23] Deb, K., & Agrawal, R. B. (1995). Simulated binary crossover for continuous search space. *Complex Systems, 9*(2), 115-148. https://www.complex-systems.com/abstracts/v09_i02_a02/

[24] Mirjalili, S., & Lewis, A. (2016). The whale optimization algorithm. *Advances in Engineering Software, 95*, 51-67. [CrossRef]

[25] Power Division, Ministry of Power, Energy and Mineral Resources. (2025). *The renewable energy policy 2025*. Government of the People's Republic of Bangladesh. Retrieved from https://objectstorage.ap-dcc-gazipur-1.oraclecloud15.com/n/axvjbnqprylg/b/V2Ministry/o/office-egcb/2026/5/0893ede8-5a55-4ce8-b575-c64468561b47.pdf



Md. Nimul Hasan received the B.Sc. degree in Electrical, Electronic and Communication Engineering (EECE) from Pabna University of Science and Technology (PUST), Pabna, Bangladesh. His research interests include hybrid renewable energy systems, microgrid operation and control, power system protection, energy management, and optimization algorithms. He has authored and co-authored several research articles in international journals and conferences on sustainable energy and optimization techniques for power systems. (Email: nimul34.din.h@gmail.com)